Supporting Information

Ti-modified $LaFeO_3$/β-SiC alveolar foams as immobilized dual catalyst with combined photo-Fenton and photocatalytic activity

Patricia García-Muñoz,[a], Fernando Fresno,[b] Christophe Lefevre,[c] Didier Robert,[a]*

*Nicolas Keller [a,]**

[a] Institut de Chimie et Procédés pour l'Energie, l'Environnement et la Santé (ICPEES), CNRS/University of Strasbourg, 25 rue Becquerel, Strasbourg, France

[b] Photoactivated Processes Unit, IMDEA Energy, Móstoles, 28935, Madrid, Spain

[c] Institut de Physique et de Chimie des Matériaux de Strasbourg (IPCMS), CNRS/University de Strasbourg, 23 rue du Loess, Strasbourg, France

corresponding authors * patricia.gmunoz@upm.es ; * nkeller@unistra.fr

Supporting Information SI1

Table S1: Concentrations of the precursors in the aqueous impregnation solution or suspension used for the incipient wetness impregnation of the β-SiC foams. Synthesis of the amorphous titania precursor.

Supporting Information SI2: Advanced X-ray diffraction (XRD) recording

Supporting Information SI3: Photonic efficiencies

Supporting Information SI4: Synthesis protocols for pristine LFO and both Ti-substituted P25-LFO and SG-LFO catalysts as powders.

Figure S1: Discretization of the foam surface into cylinders of increasing radius from the centre and irradiance received by each of these cylinders from a lamp placed at 10 cm from the external border of the foam.

Figure S2: (A) N_2 adsorption-desorption isotherms and **(B)** pore size distribution of the bare β-SiC foam support, of the reference LFO/β-SiC foam and of both P25-LFO/β-SiC and SG-LFO/β-SiC foam catalysts.

Figure S3: Observed (black), calculated (orange full line), and difference (black full line) XRD patterns of the SG-LFO/β-SiC foam catalyst recorded on a Brucker D8 Discover diffractometer (λ = 1.54056 Å), equipped with a LynxEye XE-T detector, a motorized anti-scatter screen and a Si low background sample holder for minimizing at the maximum the background noise.

Figure S4: (A) Simulated normalized intensity $I_{hkl}(LFO)/I_{112}(LFO)$ and **(B)** its relative variation as a function of the Ti → La substitution ratio within the LFO structure for selected characteristic Bragg peaks, namely (110), (111), (220) and (202). They characterize the detectability and the sensitivity of the (hkl) peak to the insertion of Ti into the LFO structure, respectively. **(C)** Simulated normalized intensity $I_{110}(LFO)/I_{112}(SiC)$ of the (110) peak of LFO for a sample consisting in a SiC matrix with 12% of LFO, the (111) peak being the most intense in the case of fcc β-SiC.

Figure S5: XPS profiles recorded on both the SG-LFO/β-SiC foam and the SG-LFO catalysts, (A) wide scan survey spectrum, (B) La 3d, (C) Fe 2p and (D) Ti 2p orbitals.

Figure S6: Time-evolution of both the C/C_0 and TOC/TOC_0 relative concentrations during the pure photocatalytic degradation of 4-CP over the P25/β-SiC foam.

Immobilization protocol for the P25/β-SiC foam

Figure S7: Evolution with time under irradiation of **(a)** the relative 4-CP concentration, **(b)** the relative TOC concentration and **(c)** the concentration of leached Fe in the solution during the combined photo-Fenton and photocatalytic degradation of 4-CP over the pristine LFO and both Ti-substituted P25-LFO and SG-LFO catalysts as powders.

Table S2: Apparent kinetic rate constants

Supporting Information SI1

Table S1: Concentrations of the precursors in the aqueous impregnation solution or suspension used for the incipient wetness impregnation of the β-SiC foams (15 mL of distilled water)

Wt.% of LFO	$La(NO_3)_3$ x $6H_2O$	$Fe(NO_3)_3$ x $9H_2O$	Citric acid	TiO_2
5 wt.%	54.2 g/L	66.5 g/L	35 g/L	-
10 wt.%	108.3 g/L	133 g/L	70g/L	6.07 g/L
20 wt.%	216.6 g/L	266g/L	140 g/L	-

Synthesis of the amorphous titania precursor:

The amorphous titania material was synthesized according to a sol-gel method under basic conditions using TTIP as precursor. In a typical synthesis, 17.8 g of TTIP was first added to a 40 mL ethanolic solution at room temperature, before a similar volume of water was added dropwise to the solution. After rectification of the pH to 9 by adding ammonia (Carlo Erba, 30% aqueous solution), the solution was left under agitation at room temperature until a dry paste was obtained. The resulting powder was further dried at 100°C for 12 h.

Supporting Information SI2

Advanced X-ray diffraction (XRD) recording

Advanced XRD recording was carried out on a Bruker D8 Discover diffractometer using a monochromatic copper radiation source with a scan step of 0.02°, and equipped with a LynxEye XE-T detector, a motorized anti-scatter screen and a Si low background sample holder for minimizing as much as possible the background noise. The Rietveld structural refinement of the SG-LFO/β-SiC foam pattern was performed with the Fullprof [1] software, using the modified Thompson-Cox-Hasting profile function (NPR = 7) for generating the line shape of the diffraction peaks. Instrumental broadening was previously determined by measuring the scattering from corundum (NIST standard SRM 1976b) [1, 2]. Simulations on the theoretical variation of the peak intensities upon Ti substitution were performed for characterizing the detectability and the sensitivity to structural Ti of the main characteristic (hkl) Bragg peaks of the LFO phase. Given that the (112) peak at 2θ=32.2° is the highest intensity peak among all the LFO (hkl) diffraction peaks, both parameters can be accessed by representing the normalized intensities (I_{hkl}/I_{112}) and their relative variations as a function of the Ti amount inserted within the structure.

[1] Rodríguez-Carvajal, J. Recent Advances in Magnetic Structure Determination by Neutron Powder Diffraction, *Physica B: Condensed Matter* **1993**, *192*, 55-69.

[2] McCusker, L. B.; Von Dreele, R. B.; Cox, D. E.; Louër, D.; Scardi, P. Rietveld refinement guidelines, *J. Appl. Cryst.* **1999**, *32*, 36-50.

Supporting Information SI3

Photonic efficiencies

In the first case, only the first electron (or hole) transfer was considered, so that the photonic efficiency was calculated as:

$$\xi_{4-CP}\ (\%) = \frac{r_{4-CP}}{\Phi} \times 100 \qquad \text{[Eq. S1]}$$

where: $\xi_{4\text{-}CP}$: photonic efficiency for 4-CP oxidation

$r_{4\text{-}CP}$: reaction rate for 4-CP oxidation ([molecules] s^{-1})

Φ : photon flux ([photons] s^{-1})

Although the degradation of 4-CP follows a complex mechanism, [1] it can be assumed that every electron withdrawn in the oxidation path down to CO_2 arises from an effectively utilized electron-hole pair upon photon absorption by the photocatalyst.[2] This can happen by direct reaction with a photo-hole, by mediation of a hydroxyl radical, or by reaction with a superoxide radical resulting from the extraction of a conduction band electron by oxygen. From a formal point of view, every 4-CP molecule converted to 6 molecules of CO_2 has lost 26 electrons, which can therefore be translated into 26 effectively used photons. The photonic efficiency for mineralization, derived from TOC disappearance can thus be defined as:

$$\xi_{TOC}\ (\%) = \frac{26 \times C_i \times V \times N_A}{\Phi \times t_{miner}} \times 100 \qquad \text{[Eq. S2]}$$

where: ξ_{TOC} : photonic efficiency for 4-CP mineralization

C_i : initial 4-CP concentration (mol L^{-1})

V : reactor volume (L)

N_A : Avogadro number (mol^{-1})

t_{miner} : time for total mineralization, ie. to achieve [TOC]= 0 (s)

Φ : photon flux (s^{-1})

For each of the two lamps used, assuming that the irradiance is constant along the lamp length, the photon flux Φ was calculated (i) from the irradiance measurements recorded at the external wall and the center of the reactor, considering that the irradiance decreases with the square of the distance from the light source, and (ii) taking into account that the foam support transmits light as determined experimentally in Figure 1 and expressed following a first order decreasing exponential model as a function of the foam radius L (Eq.S3).

$$I = I_0 \times e^{-L/0.47} \qquad \text{[Eq. S3]}$$

where I and I_0 are the transmitted and incident light, respectively, and L is the radial distance in cm from the external surface of the foam (i.e. L= 0 and L= 2.5 corresponding to the external surface and the center of the foam, respectively).

Considering this, the foam is virtually discretized as the sum of 100 concentric cylinders of increasing radius, and the photon flux Φ is obtained by numerically integrating (Figure S1) the irradiance at the external surface of those cylinders, giving a value of 7.491×10^{16} (photons) s^{-1}.

[1] Theurich, J.; Lindner, M.; Bahnemann, D. W. Photocatalytic Degradation of 4-Chlorophenol in Aerated Aqueous Titanium Dioxide Suspensions: A Kinetic and Mechanistic Study, *Langmuir* **1996**, *12*, 6368-6376.

[2] Muñoz-Batista, M. J.; Kubacka, A.; Hungría, A. B.; Fernández-García, M. Heterogeneous Photocatalysis: Light-Matter Interaction and Chemical Efects in Quantum Efficiency Calculations. *J. Catal.* **2015***, 330*, 154-166.

Supporting Information SI4

Synthesis protocol

Powdery $La_{1-x}Ti_xFeO_3$ catalysts were obtained by modifying a sol-gel Pechini synthesis. The synthesis method has been described in Garcia-Munoz et al. [1] by using two titania with distinguished crystal size and properties as titanium precursors.

The reference titanium-free $LaFeO_3$ catalyst was labelled as LFO, while the Ti-modified $LaFeO_3$ catalysts were labelled as P25-LFO and SG-LFO when using Aeroxide© TiO_2 P25 and dried amorphous titania as titanium sources, respectively. Regardless of the titanium source, the titanium added during the Pechini synthesis corresponded to a nominal amount of 10 wt% in terms of TiO_2 with respect to the theoretical amount of $LaFeO_3$ orthoferrite obtained.

[1] García-Muñoz, P.; Fresno, F.; Lefevre, C.; Robert, D.; Keller, N. Synergy Effect Between Photocatalysis and Heterogeneous PhotoFenton Catalysis on Ti-Doped $LaFeO_3$ Perovskite for High Efficiency Light-Assisted Water Treatment, *Catal. Sci. Technol.* **2020**, *10*, 1299-1310.

Figure S1

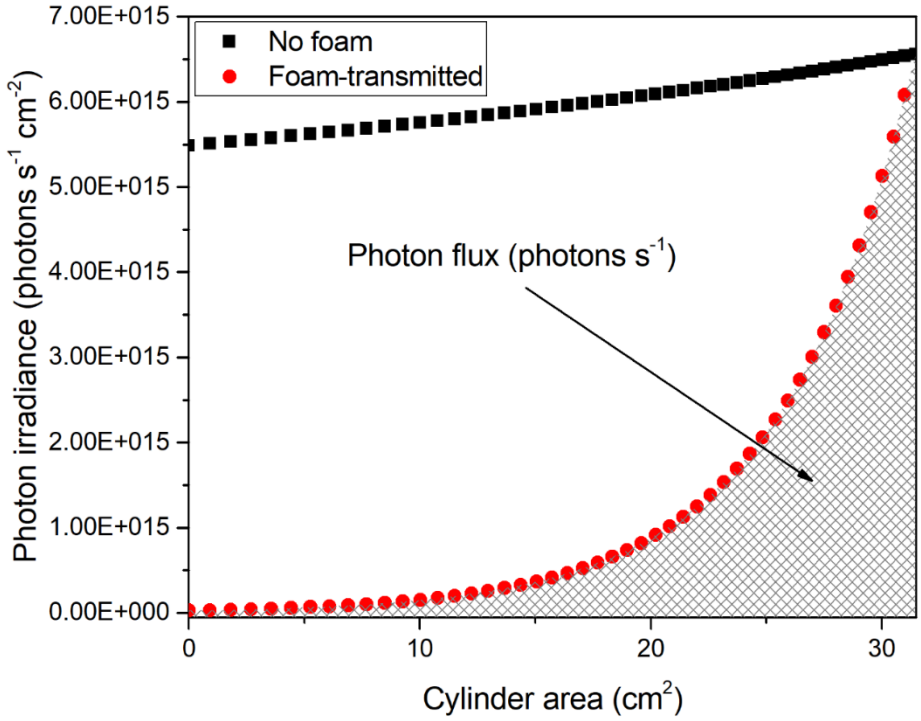

Figure S1. Discretization of the foam surface into cylinders of increasing radius from the centre and irradiance received by each of these cylinders from a lamp placed at 10 cm from the external border of the foam. The numerical integration of the irradiance curve (shaded area) gives the total amount of photons incident per unit time in the whole foam volume.

Figure S2

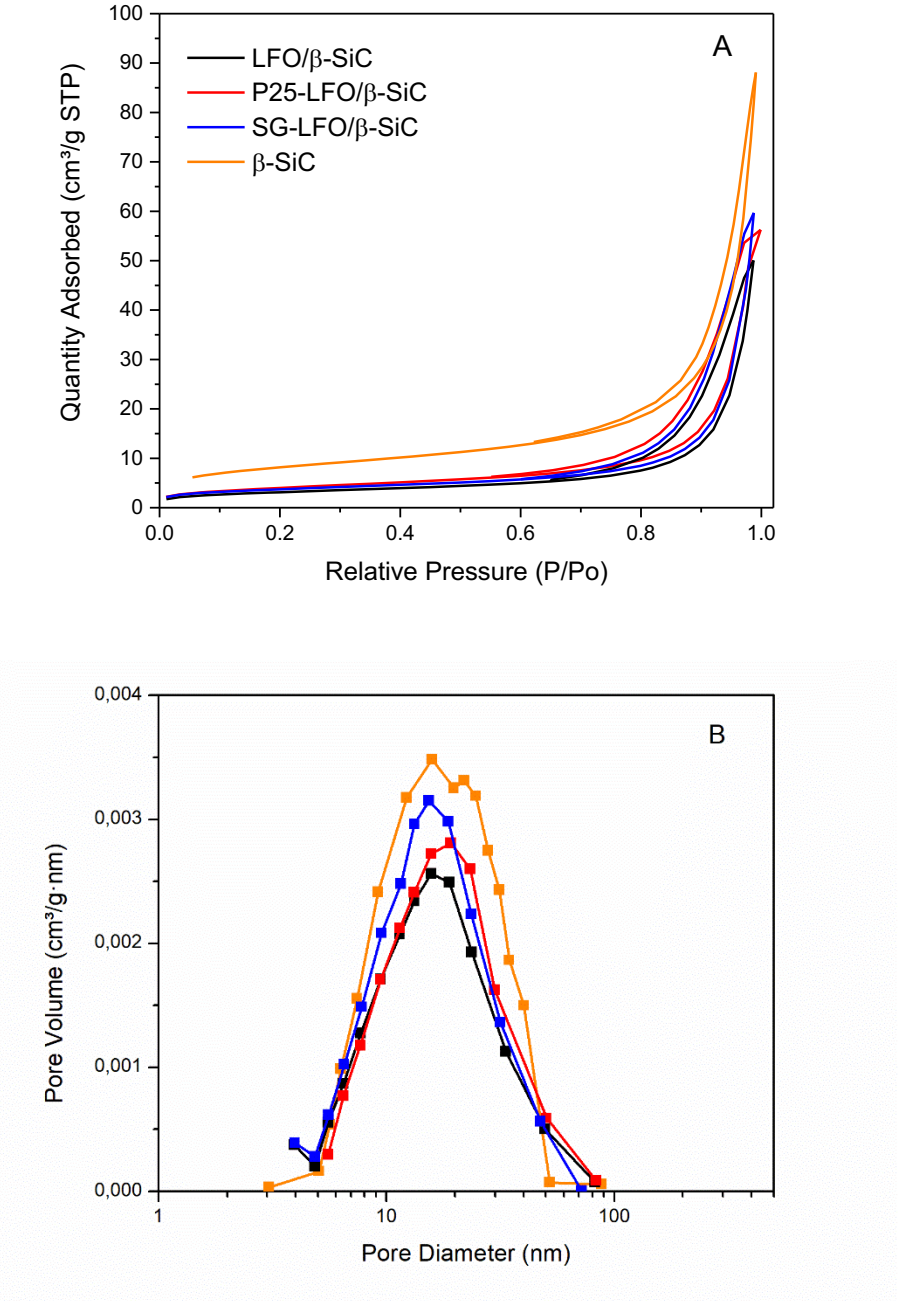

Figure S2. (A) N_2 adsorption-desorption isotherms and **(B)** pore size distribution of the bare β-SiC foam support, of the reference LFO/β-SiC foam and of both P25-LFO/β-SiC and SG-LFO/β-SiC foam catalysts.

Figure S3

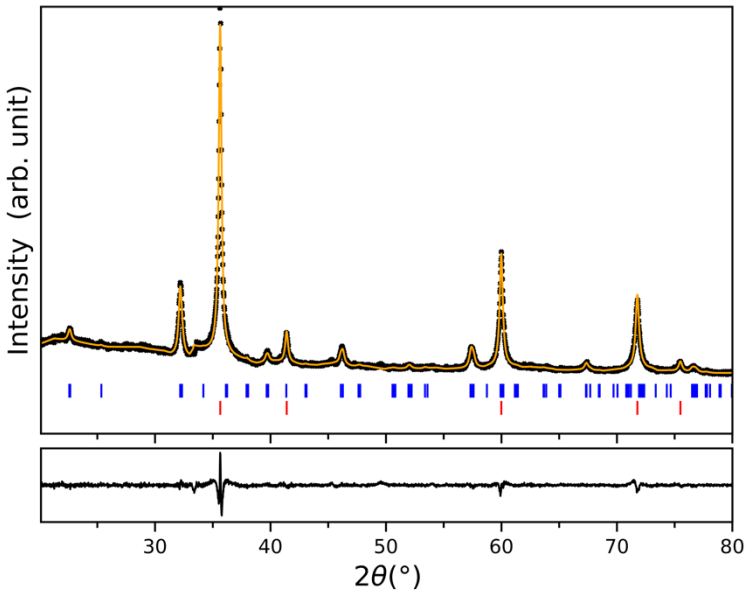

Figure S3. Observed (black), calculated (orange full line), and difference (black full line) XRD patterns of the SG-LFO/β-SiC foam catalyst recorded on a Brucker D8 Discover diffractometer (λ = 1.54056 Å), equipped with a LynxEye XE-T detector, a motorized anti-scatter screen and a Si low background sample holder for minimizing at the maximum the background noise. The positions of the Bragg reflections are represented by vertical bars, in blue for the reflexes indexed in the *Pbnm* orthorhombic unit cell of $LaFeO_3$ and in red for those of the fcc β-SiC foam support.

Figure S4

The theoretical variation of the peak intensities was computed for characterizing the detectability and the sensitivity to structural Ti of some selected characteristic Bragg peaks of the LFO phase. Both features were assessed by representing the normalized intensities (I_{hkl}/I_{112}) and their relative variations as a function of the Ti amount inserted within the structure, respectively, as shown in Figures S4A and S4B.

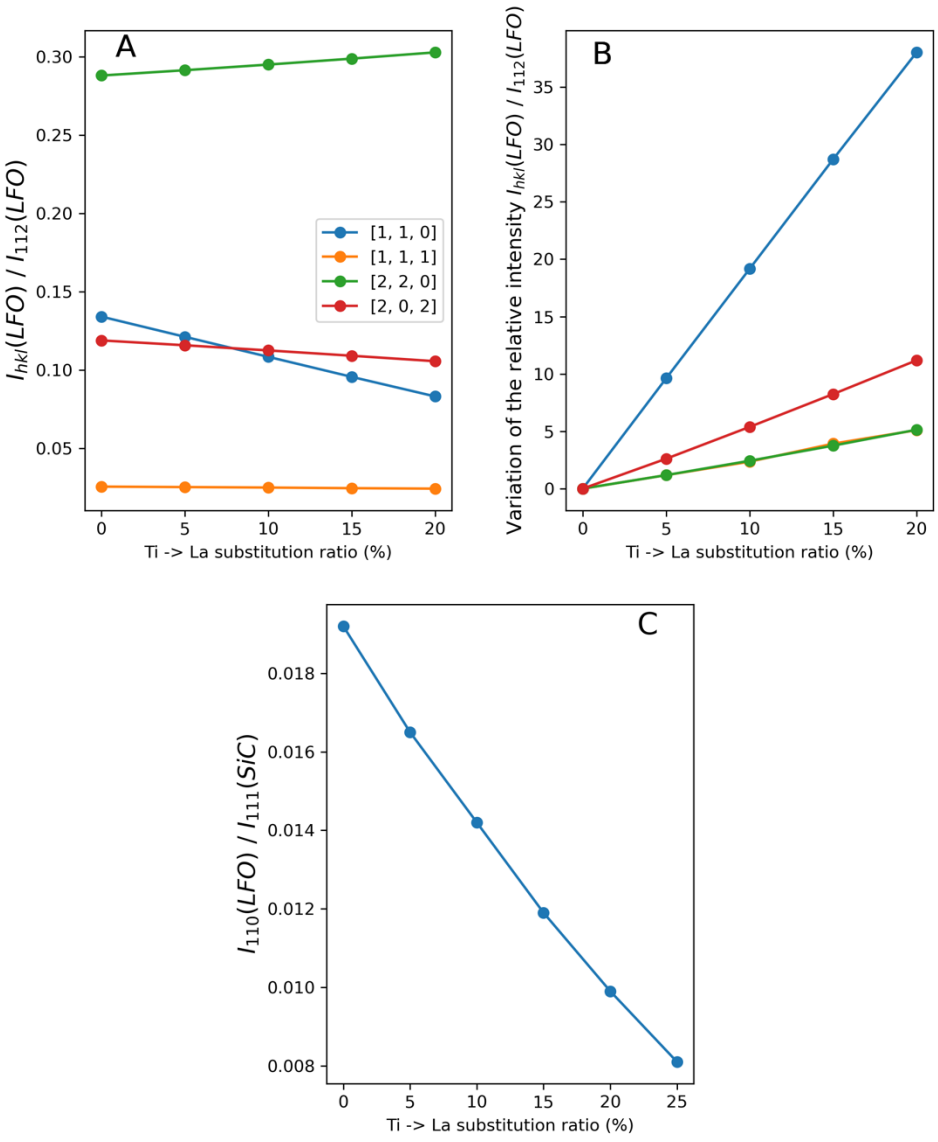

Figure S4. (A) Simulated normalized intensity I_{hkl} (LFO)/I_{112}(LFO) and **(B)** its relative variation as a function of the Ti $\rightarrow$ La substitution ratio within the LFO structure for selected characteristic Bragg peaks, namely (110), (111), (220) and (202). They characterize the detectability and the sensitivity of the (hkl) peak to the insertion of Ti into the LFO structure, respectively. **(C)** Simulated normalized intensity I_{110}(LFO)/I_{111}(SiC) of the (110) peak of LFO for a sample consisting in a SiC matrix with 12% of LFO, the (111) peak being the most intense in the case of fcc β-SiC.

Figure S5

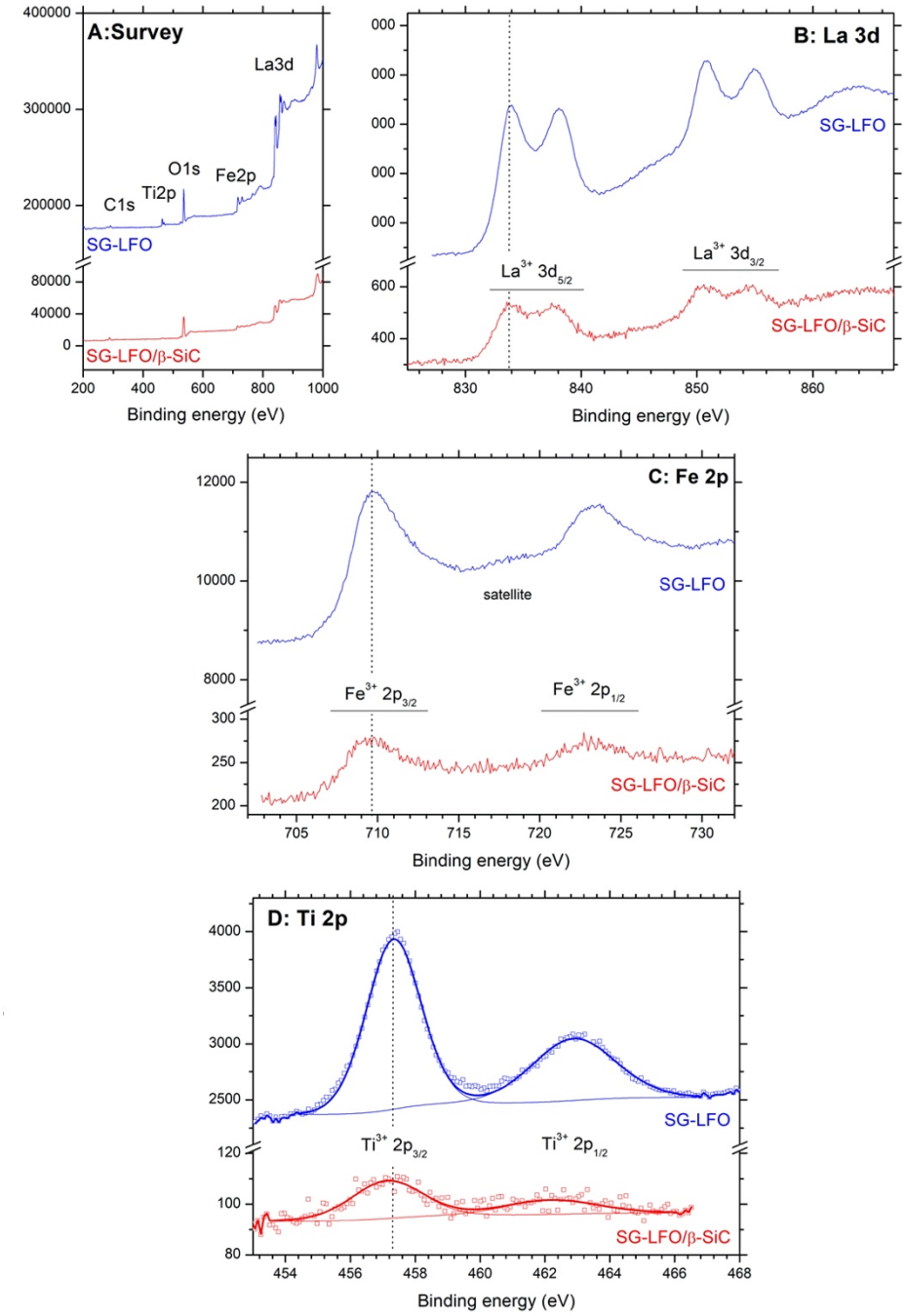

Figure S5. XPS profiles recorded on both the SG-LFO/β-SiC foam and the SG-LFO catalysts, (A) wide scan survey spectrum, (B) La 3d, (C) Fe 2p and (D) Ti 2p orbitals.

X-ray photoelectron spectroscopy (XPS) characterization was performed on a ThermoVGMultilabESCA3000 spectrometer (Al Kα anode at hλ = 1486.6 eV). The

energy shift due to electrostatic charging was subtracted using the adventitious sp2 carbon C 1s band at 284.6 eV. Contributions with Doniach–Sunjic shape and a' S-shaped' Shirley type background were used.

Figure S6

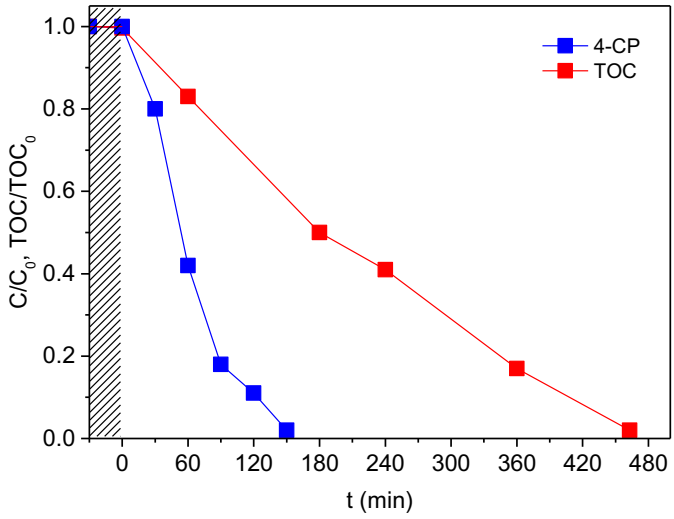

Figure S6. Time-evolution of both the C/C_0 and TOC/TOC_0 relative concentrations during the pure photocatalytic degradation of 4-CP over the P25/β-SiC foam. Conditions: $[4\text{-CP}]_0$ = 25 mg/L; T=25°C; UV-A irradiance of 60 W m^{-2}.

Immobilization protocol.

A reference β-SiC foam-supported TiO_2 catalyst with 15 wt% of Aeroxide© TiO_2 P25 was prepared via the classical deposition method consisting in successive dippings of the foam into a 15 g L^{-1} TiO_2 P25 ethanolic suspension, with intermediate rinsing steps with ethanol solution, followed by drying at 100°C and a final calcination treatment at 380°C. Prior to deposition, the bare β-SiC foam was decarboned for 2 h at 700°C in air for removing the residual unreacted carbon species by combustion. The TiO_2 content of 15 wt% relative to the total foam weight was previously optimized [1] and determined by weighing the TiO_2/β-SiC foam.

[1] Kouamé, A. N.; Masson, R.; Robert, D.; Keller, N.; Keller, V. β-SiC Foams as a Promising Structured Photocatalytic Support for Water and Air Detoxification. *Catal. Today* **2013**, *209*, 13-20.

Figure S7

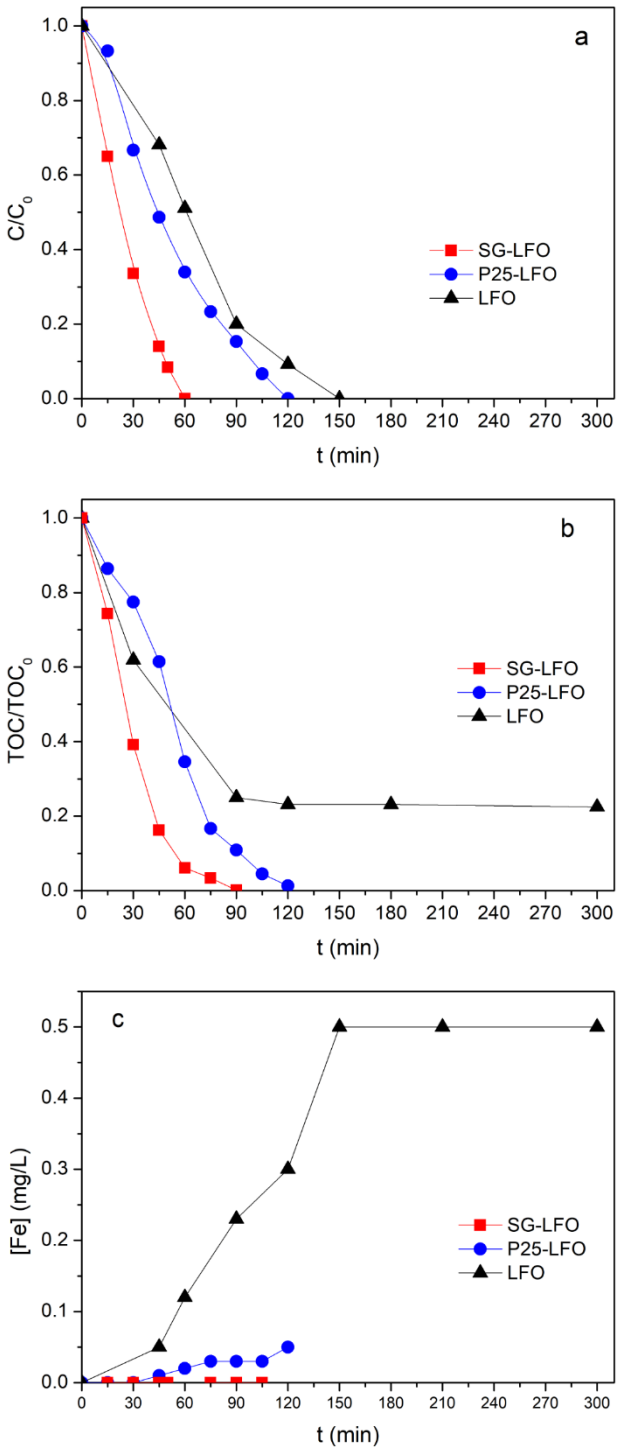

Figure S7. Evolution with time under irradiation of **(a)** the relative 4-CP concentration, **(b)** the relative TOC concentration and **(c)** the concentration of leached Fe in the solution during the combined photo-Fenton and photocatalytic degradation of 4-CP over the pristine LFO and both Ti-substituted P25-LFO and SG-LFO catalysts as powders. Conditions: $[4\text{-CP}]_0$ = 25 mg/L; $[H_2O_2]_0$ = 125 mg/L; T=25°C; [cat] = 0.5 g/L; UV-A

irradiance of 60 W m^{-2}. Data taken from Garcia-Munoz et al. and graphs adapted with permission from RSC [1].

Table S2. Apparent kinetic rate constants of 4-CP oxidation and mineralization derived from the time-evolution of the 4-CP and TOC concentrations, and concentration of Fe leached at the end of the test. Data taken from Garcia-Munoz et al. and Table adapted with permission from RSC [1].

Catalyst	k(4-CP), min^{-1}	r_0(TOC), mg L^{-1} min^{-1}	[Fe] leached, mg L^{-1}
LFO	0.020	0.12	0.5
P25-LFO	0.017	0.18	0.05
SG-LFO	0.033	0.28	<0.001

[1] García-Muñoz, P.; Fresno, F.; Lefevre, C.; Robert, D.; Keller, N. Synergy Effect Between Photocatalysis and Heterogeneous PhotoFenton Catalysis on Ti-Doped $LaFeO_3$ Perovskite for High Efficiency Light-Assisted Water Treatment, *Catal. Sci. Technol.* **2020**, *10*, 1299-1310.